Open access • Posted Content • DOI:10.1101/470096

Chondroitin sulfate proteoglycan Windpipe modulates Hedgehog signaling in Drosophila — Source link

Masahiko Takemura, Fredrik Noborn, Jonas Nilsson, Eriko Nakato ...+3 more authors

Institutions: University of Minnesota, University of Gothenburg

Published on: 14 Nov 2018 - bioRxiv (Cold Spring Harbor Laboratory)

Topics: Smoothened, Hedgehog signaling pathway and Chondroitin sulfate proteoglycan

Chondroitin sulfate proteoglycan Windpipe modulates Hedgehog signaling in *Drosophila*

[1]Masahiko Takemura, [2]Fredrik Noborn, [2]Jonas Nilsson, [1]Eriko Nakato, [1]Tsu-Yi Su, [2]Göran Larson, and [1]Hiroshi Nakato

1 Department of Genetics, Cell Biology, and Development, University of Minnesota, Minneapolis, MN, USA
2 Department of Clinical Chemistry and Transfusion Medicine, Institute of Biomedicine, University of Gothenburg, Gothenburg, Sweden

Abstract

Proteoglycans, a class of carbohydrate-modified proteins, often modulate growth factor signaling on the cell surface. However, the molecular mechanism by which proteoglycans regulate signal transduction is largely unknown. In this study, using a recently-developed glycoproteomic method, we found that Windpipe (Wdp) is a novel chondroitin sulfate proteoglycan (CSPG) in *Drosophila*. Wdp is a single-pass transmembrane protein with leucin-rich repeat (LRR) motifs and bears three CS sugar chain attachment sites in the extracellular domain. Here we show that Wdp modulates the Hedgehog (Hh) pathway. Overexpression of *wdp* inhibits Hh signaling in the wing disc, which is dependent on its CS chains and the LRR motifs. Conversely, loss of *wdp* leads to the upregulation of Hh signaling. Furthermore, knockdown of *wdp* increase the cell surface accumulation of Smoothened (Smo), suggesting that Wdp inhibits Hh signaling by regulating Smo stability. Our study demonstrates a novel role of CSPG in regulating Hh signaling.

Introduction

Spatial and temporal regulation of growth factor signaling pathways is essential to proper development and disease prevention. Cell surface signaling events, such as ligand-receptor interactions, are often modulated by proteoglycans (D. Xu & Esko, 2014). Proteoglycans are carbohydrate-modified proteins that are found on the cell surface and in the extracellular matrix. They are composed of a core protein and one or more glycosaminoglycans (GAGs) covalently attached to specific serine residues on the core protein. GAGs are long, unbranched, and highly sulfated polysaccharide chains consisting of a repeating disaccharide unit. Based on the composition of the disaccharide units, proteoglycans are classified into several types, including heparan sulfate proteoglycans (HSPGs) and chondroitin sulfate proteoglycans (CSPGs).

HSPGs function as co-receptors by interacting with a wide variety of ligands and modulate signaling activities (Holt & Dickson, 2005; J.-S. Lee & Chien, 2004; Lindahl & Li, 2009; Poulain & Yost, 2015; D. Xu & Esko, 2014). *Drosophila* offers a powerful model system to study the functions of HSPGs *in vivo* because of its sophisticated molecular genetic tools and minimal genetic redundancy in genes encoding core proteins and HS synthesizing/modifying enzymes (Lander & Selleck, 2000; Nakato & Li, 2016; Perrimon & Bernfield, 2000; Takemura & Nakato, 2015). *In vivo* studies using the *Drosophila* model have shown that HSPGs orchestrate information from multiple ligands in a complex extracellular milieu and sculpt the signal response landscape in a tissue {Nakato & Li, 2016}. However, the molecular mechanisms of co-receptor activities of HSPGs still remain a fundamental question. Our previous studies predict that there are unidentified molecules involved in the molecular recognition events on the cell surface (Akiyama et al., 2008).

In addition to HS, *Drosophila* produces CS, another type of GAG (Toyoda, Kinoshita-Toyoda, & Selleck, 2000). CSPGs are well known as major structural components of the extracellular matrix. CSPGs have also been shown to modulate signaling pathways, including Hedgehog (Hh), Wnt, and fibroblast growth factor signaling (Cortes, Baria, & Schwartz, 2009; Townley & Bülow, 2018). Given the structural similarities between CS and HS, CSPGs may have modulatory, supportive and/or complementary functions to HSPGs. However, the mechanisms by which CSPGs function as a co-receptor are unknown. In contrast to a large number of studies on HSPGs, very few CSPGs have been identified and analyzed in *Drosophila* (Momota, Naito, Ninomiya, & Ohtsuka, 2011). Unlike HSPGs, CSPG core proteins are not well conserved between species (Olson, Bishop, Yates, Oegema, & Esko, 2006). Therefore, the identification of CSPGs cannot rely on the sequence homology to mammalian counterparts.

Recently, we have developed a glycoproteomic method to identify novel proteoglycans (Noborn et al., 2016; 2018; 2015). Briefly, this method includes trypsinization of protein samples, followed by enrichment of glycopeptides using strong anion exchange (SAX) chromatography. After enzymatic digestion of HS/CS chains, the glycopeptides bearing a linkage glycan structure common to HS and CS chains are identified using nano-liquid chromatography-tandem mass spectrometry (nLC-MS/MS). This method has successfully identified novel CSPGs in humans (Noborn et al., 2015) and *Caenorhabditis elegans* (Noborn et al., 2018).

To study the function of CSPGs in signaling, we applied the glycoproteomic method to identify previously unrecognized CSPGs in *Drosophila*. We found that Windpipe (Wdp) is a novel CSPG and affects Hh signaling. Overexpression of *wdp* inhibits Hh signaling in the wing disc. This inhibitory effect of Wdp on Hh signaling is dependent on its CS chains and LRR motifs. Consistent with the overexpression analysis, loss of *wdp* increases Hh signaling. Loss of *wdp* also increases cell surface accumulation of Smoothened (Smo), the Hh signaling transducer. Therefore, we propose that Wdp downregulates Hh signaling by disrupting cell surface accumulation of Smo.

Results

A glycoproteomic approach identified Wdp as a novel *Drosophila* CSPG

We investigated the potential presence of CSPGs in *Drosophila* using our recently-developed glycoproteomic approach that identifies core proteins and its CS attachment sites. A general workflow for the sample preparation, CS-glycopeptide enrichment, LC-MS/MS analysis and the subsequent data analysis is shown in Fig. 1A. Brifely, *Drosophila* third-instar larvae were collected from two different genotypes (wild type [Oregon-R] and a loss-of-function mutant for *tout-velu* [ttv^{524}]) and the material was homogenized in ice-cold acetone. *ttv* encodes a *Drosophila* HS polymerase, and *ttv* mutants lack HS chains (Toyoda et al., 2000). The samples were incubated with trypsin and then passed over an anion exchange column equilibrated with a low-salt buffer. This procedure enriches for CS-attached glycopeptides as the matrix retains anionic polysaccharides and their attached peptides, whereas neutral or positively charged peptides flow through the column. The bound structures were eluted stepwise with three buffers of increasing sodium chloride concentrations. The resulting fractions were treated with chondroitinase ABC. This procedure reduces the lengths of the CS chains and generates a residual hexasaccharide structure still attached to the core protein. The chondroitinase-treated fractions were analyzed with positive mode nLC-MS/MS and an automated search strategy was used to identify CS modified peptides in the generated data set (Noborn et al., 2015).

The analysis revealed the Windpipe (Wdp) protein as a novel CSPG, which was modified with three CS-polysaccharides on two unique peptides (Fig. 1B and 1C). We detected Wdp glycopeptides from both wild-type and *ttv* mutant samples, further supporting that Wdp bears CS chains, not HS. One of the identified precursor ions (*m/z* 983.38; 3+) equated to the mass of a peptide with a SDQVEGSGDLSETNMELK sequence, derived from the middle part of the protein (amino acids 276–293) (Fig. 1B). The peptide was modified with one hexasaccharide structure and one methionine oxidation. The measured mass (2947.1186 Da) deviated - 3.27 ppm from the theoretical value. The other identified precursor ion (*m/z* 1276.76; 4+) equated to the mass of a peptide with a EEHIVKDEDEDDEGSGSGGGLLIIPDPSK sequence, located in proximity to the previous peptide (amino acids 320–348) (Fig. 1C). The peptide was found to be modified with two hexasaccharide structures and where one of the hexasaccharides were modified with one phosphate modification. The measured mass (5102.9389 Da) deviated +3.05 ppm from the theoretical value. Detailed inspection of the spectra revealed several b- and y-ions as well as the prominent diagnostic oxonium ion at *m/z* 362.1, corresponding to the disaccharide $[GlcAGalNAc\text{-}H_2O+H]^+$ (Fig. 1B and 1C). Furthermore, one of the glycans in Fig 1C was found modified with one phosphate group at a xylose residue (peptide + xylose + phosphate, *m/z* 1625.70; 2+).

Wdp is a single-pass transmembrane protein containing four leucine rich repeat (LRR) motifs in the extracellular domain (Huff, Kingsley, Miller, & Hoshizaki, 2002). The three CS attachment sites (S282, S334, and S336) revealed by our glycoproteomic analysis are located in the extracellular domain (Fig. 3A). Interestingly, a recent study reported that Wdp negatively regulates JAK–STAT signaling by promoting internalization and lysosomal degradation of the Domeless (Dome) receptor (W. Ren et al., 2015). We further investigated the role of Wdp, a novel CSPG, in signal transduction.

Overexpression of *wdp* inhibits Hh signaling

The growth and patterning of the *Drosophila* wing are controlled by multiple signaling pathways, including Decapentaplegic (Dpp; the *Drosophila* BMP), Wingless (Wg; the *Drosophila* Wnt), and Hedgehog (Hh) signaling (Baena-Lopez, Nojima, & Vincent, 2012; Tabata & Takei, 2004). To determine the role of *wdp* in these developmental signaling pathways, we first asked whether overexpression of *wdp*

affects adult wing morphology. When *wdp* was overexpressed in the wing pouch using Bx^{MS1096}-*GAL4* (Capdevila & Guerrero, 1994) (Bx^{MS1096}>*wdp*), the wing size was reduced compared to that of control flies (Bx^{MS1096}>) (Fig. 3C; compared to Fig. 3B). In addition, the distance between longitudinal wing veins 3 and 4 (L3 and L4) was aberrantly narrower. This decreased distance between L3 and L4 is indicative of reduced Hh signaling during wing development (Mullor, Calleja, Capdevila, & Guerrero, 1997; Strigini & Cohen, 1997).

Hh is produced in the posterior compartment of the wing disc and spreads towards the anterior compartment where Hh signaling induces target genes expression in a concentration-dependent manner (Briscoe & Thérond, 2013; Gradilla & Guerrero, 2013; Hartl & Scott, 2014). Expression of high-threshold target genes, such as Patched (Ptc; the Hh receptor) (Capdevila, Pariente, Sampedro, Alonso, & Guerrero, 1994) and Engrailed (En) (Patel et al., 1989) are induced in anterior cells near the anteroposterior compartment boundary by high levels of Hh signaling (Jia, Tong, Wang, Luo, & Jiang, 2004) (Fig. 2A and 2E). Low levels of Hh signaling induce the expression of *dpp* and the accumulation of full-length Cubitus interruptus (Ci; the transcriptional factor of Hh signaling) in a broader region (more distant away from the anteroposterior boundary) (Fig. 2A and 2C). To determine if Hh signaling is indeed affected by *wdp*, we overexpressed *wdp* in the dorsal compartment of the wing disc using *ap-GAL4* (Calleja, Moreno, Pelaz, & Morata, 1996; O'Keefe, Thor, & Thomas, 1998). We found that *wdp* overexpression in the dorsal compartment reduced the expression domains of both "high-threshold" targets (Ptc and En) and "low-threshold" targets (*dpp-lacZ*^{10638}, a reporter for *dpp* expression, and full-length Ci) compared to those in the ventral compartment (Fig. 2B, 2D, and 2F). Notably, overexpression of *wdp* did not affect the pattern of a *hh* transcriptional reporter *hh-lacZ*^{P30} (J. J. Lee, Kessler, Parks, & Beachy, 1992) (Fig. 2F). Together, *wdp* acts as a negative regulator of Hh signaling without affecting *hh* transcription

On the other hand, Wdp does not appear to affect Dpp and Wg pathways. When *wdp* is overexpressed using *ap-GAL4* or *hh-GAL4* (a posterior compartment-specific GAL4 driver) (Tanimoto, Itoh, Dijke, & Tabata, 2000), we did not observe apparent defects in Dpp signaling activity, which was monitored by the expression of phosphorylated Mad (pMad) and Spalt major (Salm) (readouts of Dpp signaling). Similarly, no changes in expression of Senseless (Sens) and Distal-less (Dll) (readouts of Wg signaling) were detected (Fig. S1). These results are consistent with a previous report (W. Ren et al., 2015).

We also found that overexpression of *wdp* induces massive apoptosis, as detected with anti-cleaved Caspase-3 antibody (Fig. S2B). This likely contributed to the smaller adult wing phenotype observed in Bx^{MS1096}>*wdp* flies. It was recently reported that Hh signaling is required for cell survival in wing disc cells (Lu, Wang, & Shen, 2017). To determine whether reduced Hh signaling is responsible for the observed apoptosis, we first asked if reduced Hh signaling results in apoptosis. We inhibited Hh signaling either by expressing an RNAi construct targeting *smo* (TRiP.HMC03577) (Fig. S2E), or by overexpressing *ptc* in the dorsal compartment using *ap-GAL4*. We found that neither treatment caused massive apoptosis (Fig. S2F and S2G), indicating that reduced Hh signaling is not sufficient to induce massive apoptosis in the wing disc. Furthermore, coexpression of a constitutively active form of Smo with Wdp did not suppress apoptosis in the wing disc (Fig. S2H). Thus, these results suggest that overexpression of *wdp* induces apoptosis, independent of reduced Hh signaling.

CS and LRR motifs are necessary for Wdp to inhibit Hh signaling

Next, we asked whether the CS chains of Wdp are required for its function. In a CSPG core-protein, CS is attached to specific serine residues in the consensus serine-glycine dipeptide surrounded by acidic amino acids (Esko & Zhang, 1996). We generated a *UAS-wdp*$^{\Delta GAG}$ construct in which all three serine residues (S282, S334, and S336) are substituted with alanine residues so that CS cannot be attached to the core

protein (Fig. 3A). The *UAS-wdp*$^{\Delta GAG}$ construct was inserted in the same genomic location (ZH-86Fb; (Bischof, Maeda, Hediger, Karch, & Basler, 2007)) as *UAS-wdp* using the *phiC31* site-specific integration system (Groth, Fish, Nusse, & Calos, 2004) in order to ensure the same expression level of the UAS transgenes.

We found that *Bx*^{MS1096}>*wdp*$^{\Delta GAG}$ adult wings did not display the reduction in the distance between L3 and L4 (Fig. 3B). Consistent with this, the expression of Ptc, En, Ci, and *dpp-lacZ* in the wing disc were not affected by *wdp*$^{\Delta GAG}$ overexpression in the dorsal compartment of the wing disc (Fig. 3E–G). These results indicate that CS chains are required for Wdp's activity to downregulate Hh signaling.

To determine whether the LRR motifs and/or the intracellular domain of Wdp are necessary for inhibiting Hh signaling, we generated several Myc-tagged mutant constructs (Fig. S3) and examined their activities. Consistent with the earlier result (Fig. 2B), expression of a Myc-tagged Wdp (Myc:Wdp) led to the narrower Ptc expression domain (Fig. 3G). A mutant *wdp* construct lacking LRR motifs (Myc:Wdp$^{\Delta LRRs}$) failed to inhibit Hh signaling (Fig. 3H). On the other hand, a truncated construct lacking the intracellular domain (Myc:Wdp$^{\Delta ICD}$) retained the ability to inhibit Hh signaling (Fig. 3I). Thus, in addition to CS chains, the LRR motifs of Wdp are required for inhibiting Hh signaling.

Wdp expression in the wing disc

To monitor Wdp expression, we generated transgenic flies (*wdp*$^{KI.HA}$ and *wdp*$^{KI.OLLAS}$) expressing epitope-tagged Wdp protein from its endogenous locus. We inserted a spaghetti monster GFP with 10 copies of HA or OLLAS tags (Nern, Pfeiffer, & Rubin, 2015; Viswanathan et al., 2015) near the C-terminus of Wdp (after Q652; Fig. 4A) using CRISPR–Cas9-mediated homology-directed repair (Gratz et al., 2014; X. Ren et al., 2014). The Wdp:HA expression was detected in the eye disc, adult midgut, and tracheal system (Fig. S3), consistent with previous reports (Huff et al., 2002; W. Ren et al., 2015).

In the wing disc, Wdp:HA is expressed in most of the wing disc cells with enrichment in the basal side, as detected by anti-HA antibody (Fig. 4B and 4C). This result was confirmed by anti-OLLAS antibody staining of the *wdp*$^{KI.OLLAS}$ wing discs (Fig. S3A and S3B). In the wing disc epithelium, mitotic nuclei apically translocate, but the cells maintain contact with the basal lamina via actin-rich basal projection (Ragkousi & Gibson, 2014). Interestingly, Wdp:HA is strongly enriched in such basal projections (Fig. 4A and 4D). However, physiological significance of this localization of Wdp in the basal projections of mitotic cells is unknown.

Loss of *wdp* leads to higher levels of Hh signaling

To determine whether loss of *wdp* affects Hh signaling activity, we examined the effect of *wdp* RNAi knockdown in the wing disc. Expression of a *wdp*^{RNAi} construct (TRiP.HMC06302) using *ap-GAL4* in *wdp*$^{KI.HA/+}$ flies led to the loss of Wdp:HA staining specifically in the dorsal compartment (Fig. 4E), validating the efficacy of RNAi-mediated knockdown of *wdp*. We then examined the effect of *wdp* knockdown on Hh signaling using the Ptc expression level as a readout of the Hh signaling activity. In control wing discs (*ap>FLP*), the signal intensity of Ptc staining in the dorsal compartment is comparable to that in the ventral compartment (Fig. 5B). On the other hand, *wdp*^{RNAi} expression using *ap-GAL4* increased the signal intensity of Ptc staining only in the dorsal compartment (Fig. 5A and 5C). In addition, we observed that the *dpp-lacZ* expression domain was expanded anteriorly by *wdp* knockdown (Fig. 5D). In the adult wing, knockdown of *wdp* slightly expanded the distance between wing vein L3 and L4 near the distal tip (Fig. 5J, compared to Fig. 5I). Thus, *wdp* RNAi knockdown results in a moderate increase in Hh signaling.

To confirm the *wdp* knockdown phenotypes, we generated a loss-of-function allele of *wdp* ($wdp^{KO.\Delta CDS}$), in which most of the *wdp* coding sequence was removed using CRISPR–Cas9-mediated defined deletion (Gratz et al., 2013) (Fig. 5E–G). $wdp^{KO.\Delta CDS}$ homozygous mutant clones were induced in the wing pouch using the FLP–FRT system with *nubbin (nub)-GAL4 UAS-FLP* and their effect on Hh signaling was examined using anti-Ptc antibody. Consistent with the RNAi knockdown results, we observed a modest increase of Ptc expression in cells mutant for *wdp* (Fig. 5H). Taken together, we conclude that *wdp* negatively regulates Hh signaling in the *Drosophila* wing.

Wdp inhibits Smo cell surface accumulation

The seven-pass transmembrane protein Smo is a key transducer of Hh signaling. In the absence of Hh, Ptc inhibits the phosphorylation of Smo, which is internalized and degraded (Zhu, Zheng, Suyama, & Scott, 2003). In the presence of Hh, restriction of Ptc on Smo is relieved, allowing Smo to accumulate on the cell surface and activate Hh signaling. Although *smo* transcription is ubiquitous, Smo protein expression levels are high in the posterior compartment of the wing disc where Ptc is not expressed (Fig. 6A) (Denef, Neubüser, Perez, & Cohen, 2000). We found that knockdown of *wdp* increases the cell surface accumulation of Smo (Fig. 6B). This result suggests that Wdp downregulates Hh signaling either by disrupting Smo translocation to the cell membrane or the stability of Smo on the cell surface.

Discussion

The molecular mechanism by which HSPG co-receptors regulate growth factor signaling remains a central question in cell biology. Dally, a *Drosophila* HSPG of the glypican type, potentiates Dpp signaling by stabilizing the ligand-receptor complex on the cell surface (Akiyama et al., 2008), suggesting that controlling the rate of receptor-mediated internalization of the signaling complex is the basis for co-receptor activity. However, it is still unknown how HSPGs affect endocytosis and internalization. Since glypicans do not have an intracellular domain, it is likely that these molecules cooperate with other factors (e.g. membrane proteins) to exert co-receptor activity. Thus, it is clear that there are many more unknown factors involved in molecular recognition events on the cell surface. To understand the molecular basis for cell communications, it is critical to identify novel cell surface players.

We found that in the wing disc, Wdp negatively regulates Hh signaling in a CS- and LRR motif-dependent manner. It has also been reported that Wdp negatively regulates JAK–STAT signaling and controls adult midgut homeostasis and regeneration (W. Ren et al., 2015). The authors showed that Wdp interacts with the Dome receptor and promotes its endocytosis and lysosomal degradation. Thus, it is interesting to test if Wdp interacts with Dome via CS chains to modulate JAK–STAT signaling. We observed that Wdp affects cell surface accumulation of Smo, suggesting its role in regulating the stability of Smo protein. Thus, it is possible that Wdp modulates these pathways via a similar mechanism: controlling the internalization of Dome and Smo on the cell membrane.

It is worth noting that both JAK–STAT and Hh signaling, the two pathways negatively controlled by Wdp, are also regulated by HSPGs. Dally-like, a glypican family of HSPGs, positively regulates Hh signaling by interacting with Hh and Ptc (Desbordes & Sanson, 2003; M.-S. Kim, Saunders, Hamaoka, Beachy, & Leahy, 2011; Lum, Yao, et al., 2003a; Williams et al., 2010; Yan et al., 2010). In the developing ovary, Dally upregulates the JAK–STAT pathway (Y. Hayashi et al., 2012). Given the importance of precise dosage control of oncogenic pathways, such as JAK–STAT and Hh signaling, this dual proteoglycan system could play an important role in fine-tuning of the signaling output in order to prevent cancer formation. In vertebrates, HSPGs and CSPGs show opposing effects in neural systems. For example, axon growth is typically promoted by HSPGs but inhibited by CSPGs (Bandtlow & Zimmermann, 2000; Coles et al., 2011; Kantor et al., 2004; Matsumoto, Irie, Inatani, Tessier-Lavigne, & Yamaguchi, 2007; Silver & Miller, 2004; Van Vactor, Wall, & Johnson, 2006). Our findings suggest that such competing effects of HSPGs and CSPGs may be a general mechanism for the precise control of signaling cascades and pattern formation.

In addition to the functions in signaling, Wdp may play other roles. We found that overexpression of *wdp* results in massive apoptosis in the wing disc, independent of Hh signaling inhibition (Fig. S2). Since CSPGs are well known for structural functions, an excess amount of Wdp may affect the epithelial integrity of the wing disc, leading to subsequent apoptosis. Our observation that Wdp is enriched on the basal side of the wing disc and adult midgut cells (Fig. 4B and S3F) suggests that Wdp may interact with components of the basement membrane, which surrounds these organs.

In mice, sulfated CS is necessary for Indian hedgehog (Ihh) signaling in the developing growth plate (Cortes et al., 2009). Ihh and Sonic hedgehog (Shh) bind to CS (Cortes et al., 2009; Whalen, Malinauskas, Gilbert, & Siebold, 2013; F. Zhang, McLellan, Ayala, Leahy, & Linhardt, 2007). Thus, it will be interesting to check if Wdp interacts with Hh via its CS chains.

Previous studies also reported that *wdp* is associated with aggressive behaviors in *Drosophila* species. *wdp* is upregulated in the head of socially isolated male flies, which exhibit more aggressive behaviors than males raised in groups (L. Wang, Dankert, Perona, & Anderson, 2008). Also, *wdp* expression is slightly higher in the brain of *Drosophila prolongata*, which is more aggressive compared to its closely-

303 related species (Kudo et al., 2017). Since CSPGs are important in neuronal patterning (Saied-Santiago &
304 Bülow, 2018), it is interesting to study the molecular mechanisms behind Wdp's effect on *Drosophila*
305 behavior.
306
307 In mammals, there are a class of CSPG molecules with LRR motifs (small leucine-rich proteoglycans, or
308 SLRPs). A number of SLRP members are known as causative genes of human genetic disorders (Bech-
309 Hansen et al., 2000; Pusch et al., 2000; Schaefer & Iozzo, 2008). Although Wdp does not have cysteine-
310 rich regions that are commonly found in mammalian SLRPs, MARRVEL (ver 1.1) (J. Wang et al., 2017)
311 reports that *wdp* is a potential *Drosophila* ortholog of the human *NYX* gene (nyctalopin), a member of
312 SLRPs (DIPOT score 1 (Hu et al., 2011)). Mutations in *NYX* cause X-linked congenital stationary night
313 blindness (Bech-Hansen et al., 2000; Pusch et al., 2000). Further studies on Wdp will provide a novel
314 insight into the function of these disease-related human counterparts.
315
316

Materials and Methods

Preparation of glycosaminoglycan-glycopeptides and LC-MS/MS analysis

Glycosaminoglycan-glycopeptide samples were prepared from wild-type (Oregon-R) and *ttv* mutant (*ttv*^{524}) third-instar larvae as previously described (Noborn et al., 2015; 2018). Briefly, 200-400 third instar larvae (wet weight; 200-400 mg) were lyophilized and homogenized using a motor pestle in 1 ml of ice-cold acetone. After extensive washes with acetone, the insoluble fraction was recovered by centrifugation. After overnight desiccation, the pellet was dissolved in 1.5 ml 1% CHAPS lysis buffer and boiled for 10 min at 96°C. The sample was adjusted to 2 mM $MgCl_2$ and incubated with 3 µl Benzonase (MilliporeSigma, Burlington, MA) at 37°C for three hours. After heat-inactivation of Benzonase, the sample was centrifuged and the supernatant was collected in a new tube.

An aliquot of the preparation (1 mg of protein) was further used. The sample was reduced and alkylated in 1 ml 50 mM NH_4HCO_3, and trypsinized at 37°C overnight with 20 µg trypsin (Promega, Madison, WI). The digested samples were applied onto DEAE (GE Healthcare, Chicago, IL) columns (600 µl) at 4°C. The columns were washed with three different low-salt washing solutions at 4°C: 50 mM Tris-HCl, 100 mM NaCl, pH 8.0; 50 mM NaAc, 100 mM NaCl, pH 4.0; and 100 mM NaCl. The glycopeptides that were bound to DEAE were eluted stepwise with three buffers with increasing sodium chloride concentrations at 4°C: 4 ml 250 mM NaCl, 400 mM NaCl, 800 mM NaCl, and 3 ml 1500 mM NaCl. Each fraction was desalted using PD10-columns (GE Healthcare).

All fractions were lyophilized and the salt-free samples were then individually treated with 1 mU of chondroitinase ABC (Sigma-Aldrich, St. Louis, MO) for 3 h at 37°C. Prior to MS-analysis, the samples were desalted using a C18 spin column (8 mg resin) according to the manufacturer's protocol (Thermo Fisher Scientific, Waltham, MA). LC-MS/MS analysis was performed as previously described (Noborn et al., 2015; 2018). In brief, the samples were analyzed on a Q Exactive mass spectrometer coupled to an Easy-nLC 1000 system (Thermo Fisher Scientific). Briefly, glycopeptides (2-µl injection volume) were separated using an analytical column with Reprosil-Pur C18-AQ particles (Dr. Maisch GmbH, Ammerbuch, Germany). The following gradient was run at 300 nl/min; from 7-35 % B-solvent (acetonitrile in 0.2% formic acid) over 75 min, to 100 % B-solvent over 5 min, with a final hold at 100% B-solvent for 10 min. The A-solvent was 0.2% formic acid. Spectra were recorded in positive ion mode and MS scans were performed at 70,000 resolution with a mass range of *m*/*z* 600–1800. The MS/MS analysis was performed in a data-dependent mode, with the top ten most abundant charged precursor ions in each MS scan selected for fragmentation (MS2) by higher energy collision dissociation with normalized collision energy values of 30. The MS2 scans were performed at a resolution of 35,000 (at *m*/*z* 200). The data analyses were performed as previously described (Noborn et al., 2015) with some small adjustments. In brief, the HCD.raw spectra were converted to Mascot .mgf format using Mascot distiller (version 2.3.2.0, Matrix Science, London, UK). The ions were presented as singly protonated in the output Mascot file. Searches were performed using an in-house Mascot server (version 2.3.02) with the enzyme specificity set to *Trypsin*, and then to *Semitrypsin*, allowing for one or two missed cleavages, in subsequent searches on *Drosophila* sequences of the UniprotKB (42, 507, sequences, 2018-06-18). The peptide tolerance was set to 10 parts per million (ppm) and fragment tolerance was set to 0.01 Da. The searches were allowed to include variable modifications at serine residues of the residual hexasaccharide structure [GlcA(-H_2O)GalNAcGlcAGalGalXyl-O-] with 0 ($C_{37}H_{55}NO_{30}$, 993.2809 Da), 1 ($C_{37}H_{55}NO_{33}S$, 1073.2377 Da), or 2 ($C_{37}H_{55}NO_{36}S_2$, 1153.1945 Da) sulfate groups attached.

Fly husbandry and fly strains, and transgenic flies

The following fly strains were used in this study:

Oregon-R, w^{1118} (Bloomington Drosophila Stock Center [BDSC] #5905), ttv^{524} (Takei, 2004), *ap-GAL4* (O'Keefe et al., 1998), *hh-GAL4* (Tanimoto et al., 2000), Bx^{MS1096}*-GAL4* (BDSC #8860) (Capdevila & Guerrero, 1994), *AB1-GAL4* (BDSC #1824) (Tavsanli et al., 2004), $elav^{C155}$*>mCD8:GFP* (BDSC #5146) (Lin & Goodman, 1994), *UAS-GFP* (BDSC #1521), *UAS-tdTomato* (BDSC #36327 and #36328), *UAS-FLP* (BDSC #4539 and #4540), *UAS-ptc* (BDSC #44614), *nub-GAL4* (BDSC #25754), *FRT42D 2xUbi-GFP*, *UAS-smo:GFP* (BDSC #44624), *UAS-FLAG:smo*^{Act} (BDSC #44621), *UAS-wdp*^{RNAi} (TRiP.HMC06302, BDSC #66004), *UAS-wdp*^{RNAi} (TRiP.HM05118, BDSC #28907), *UAS-smo*^{RNAi} (TRiP.HMC03577, BDSC #53348), *hh-lacZ*^{P30} (a gift from Gary Struhl) (J. J. Lee et al., 1992), *dpp-lacZ*^{10638} (BDSC #12379) (Zecca, Basler, & Struhl, 1995), *vas-Cas9* (BDSC #55821), *esg-GAL4* (DGRC #113886) (S. Hayashi et al., 2002). The *UAS-wdp*, *UAS-wdp*$^{\Delta GAG}$, *UAS-Myc:wdp*, *UAS-Myc:wdp*$^{\Delta LRRs}$, *UAS-Myc:wdp*$^{\Delta ICD}$, *wdp*$^{KO.\Delta CDS}$, *wdp*$^{KI.HA}$, *wdp*$^{KI.OLLAS}$ flies were generated in this study. A full list of genotypes used in this study can be found in Table S1.

For constructing *UAS-wdp*, *wdp* CDS (corresponding to wdp-RA–E in FlyBase) was inserted into the XhoI- and XbaI-digested pJFRC7 vector (a gift from Gerald Rubin; Addgene # 26220) (Pfeiffer et al., 2010) using NEBuilder HiFi DNA Assembly Master Mix (New England Biolabs [NEB], Ipswich, MA, E2621S). Similarly, *wdp*$^{\Delta GAG}$ (S282A, S334A, and S336A), *Myc:wdp*, *Myc:wdp*$^{\Delta LRRs}$, and *Myc:wdp*$^{\Delta ICD}$ were inserted into the pJFRC7 vector. The UAS transgenic flies were generated using *phiC31* integrase-mediated transgenesis at the ZH-86Fb attP (FBti0076525) integration site. Embryonic injection was performed by BestGene Inc (Chino Hills, CA). Primers used in this study will be available upon request.

To generate the *wdp*$^{KO.\Delta CDS}$ allele, two sgRNAs (pU6-sgRNA-wdp-1 and pU6-sgRNA-wdp-2) were introduced to delete the *wdp* CDS. To construct sgRNA plasmids, 5' - CTTCGACAGGGCCAACCAGGCGGTC - 3' and 5' - AAACGACCGCCTGGTTGGCCCTGTC - 3' were annealed (pU6-sgRNA-wdp-1); and 5' - CTTCGAGTGGCCATTGATCACCTGG - 3' and 5' - AAACCCAGGTGATCAATGGCCACTC - 3' (pU6-sgRNA-wdp-2) were annealed and ligated in the BbsI-digested pU6-BbsI-chiRNA plasmid (a gift from Melissa Harrison, Kate O'Connor-Giles, and Jill Wildonger; Addgene #45946) (Gratz et al., 2013). A mixture of 50 ng/µl of pU6-sgRNA-wdp-1 and pU6-sgRNA-wdp-2 was injected into the embryos of the *vas-Cas9* flies, which express Cas9 under the control of the germline *vasa* regulatory elements (Gratz et al., 2014), by BestGene Inc. The *wdp*$^{KO.\Delta CDS}$ allele was screened by PCR and verified by Sanger sequencing.

To generate the *wdp*$^{KI.HA}$ allele, we constructed a donor plasmid, which contained a Gly-Gly-Ser linker, smGFP-HA, and approximately 1-kb homology arms to *wdp* flanking the linker and smGFP-HA, for homology-directed repair. smGFP-HA and the *wdp* homology sequences on either side of the targeted DSB were PCR-amplified from pJFRC201-10XUAS-FRT>STOP>FRT-myr:smGFP-HA (a gift from Gerald Rubin; Addgene plasmid #63166) (Nern et al., 2015) and genomic DNA extracted from the *vas-Cas9* flies, respectively. These fragments were cloned into the pHD-DsRed-attP backbone (a gift from Melissa Harrison, Kate O'Connor-Giles and Jill Wildonger; Addgene #51019) (Gratz et al., 2014) using NEBuilder HiFi DNA Assembly Master Mix (NEB, E2621S). Similarly, we generated a donor plasmid with OLLAS tags amplified from pJFRC210-10XUAS-FRT>STOP>FRT-myr:smGFP-OLLAS (a gift from Gerald Rubin; Addgene plasmid #63170) (Nern et al., 2015). A mixture of 50 ng/µl of pU6-sgRNA-wdp-2 and 125 ng/µl of each donor plasmid was injected into the *vas-Cas9* embryos by BestGene Inc. The *wdp*$^{KI.HA}$ and *wdp*$^{KI.OLLAS}$ alleles were screened by PCR and verified by Sanger sequencing.

Flies were raised on a standard cornmeal fly medium at 25°C unless otherwise indicated.

Mosaic analysis

The *wdp*$^{KO.\ \Delta CDS}$ homozygous clones were generated by FLP/FRT-mediated mitotic recombination (T. Xu & Rubin, 1993). The FLP expression was induced by *nub-GAL4 UAS-FLP*.

Immunohistochemstry

Third-instar larval imaginal discs were stained as described previously (Takemura & Adachi-Yamada, 2011) with some modifications. Wing discs were dissected from third-instar wandering larvae in phosphate-buffered saline (PBS, pH 7.4) and subsequently fixed in 3.7% formaldehyde in PBS for 15 min at room temperature. After three 10-min washes with PBST (PBS containing 0.1% (vol/vol) Triton X-100 [Sigma, T8532]), the samples were incubated in primary antibodies overnight at 4°C. After three 10-min washes with PBST, the samples were incubated with Alexa Fluor-conjugated secondary antibodies (1:500, Thermo Fisher Scientific) overnight at 4°C or 2 hours at room temperature. After three 10-min washes with PBST, the samples were stained with 1 µg/ml DAPI (Thermo Fisher Scientific, 62248) and subsequently mounted in VECTASHIELD Antifade Mounting Medium (Vector Laboratories, Burlingame, CA, H-1000). F-actin was stained with Alexa Fluor 568 phalloidin (Thermo Fisher Scientific, A12380). Adult midguts were dissected and immunostained as previously described (Takemura & Nakato, 2017). Images were acquired on a LSM710 confocal microscope (Carl Zeiss, Oberkochen, Germany). For quantification of Ptc staining, images were acquired with the same condition, and fluorescence intensity was measured in a set area with Fiji (Schindelin et al., 2012).

Antibodies

The primary antibodies used were as follows: mouse anti-Ptc Apa 1 (1:20, Developmental Studies Hybridoma Bank [DSHB], Iowa City, IA, deposited by Isabel Guerrero) (Capdevila et al., 1994), rat anti-Ci 2A1 (1:20, DSHB, deposited by Robert Holmgren) (Motzny & Holmgren, 1995), chicken anti-β-Galactosidase (1:2000, Abcam), mouse anti-En 4D9 (1:20, DSHB, deposited by Corey Goodman) (Riggleman, Schedl, & Wieschaus, 1990), rabbit anti-pH3 (1:1000, Millipore, 06-570), rat anti-HA 3F10 (1:200, Roche, 11867423001), rabbit anti-HA C29F4 (1:1000, Cell Signaling, 3724), mouse anti-Smo 20C6 (1:50, DSHB, deposited by Philip Beachy) (Lum, Zhang, et al., 2003b), rabbit anti-pSmad3 (1:1000, Epitomics, 1880-1) (Smith, Machamer, Kim, Hays, & Marques, 2012), rabbit anti-Salm (1:30, a gift from Scott Selleck), mouse anti-Dll 1:500 (1:500, a gift from Dianne Duncan) (D. M. Duncan, Burgess, & Duncan, 1998), guinea pig anti-Sens (1:1000, a gift from Hugo Bellen) (Nolo, Abbott, & Bellen, 2000), rabbit anti-cleaved Caspase-3 (1:200, Cell Signaling, 9661), rat anti-OLLAS L2 (1:500, Novus Biologicals, NBP1-06713), mouse anti-Arm N2 7A1 (1:50, DSHB, deposited by Eric Wieschaus) (Riggleman et al., 1990), mouse anti-Pros MR1A (1:50, DSHB, deposited by C.Q. Doe) (Campbell et al., 1994), and mouse anti-Fas3 7G10 (1:50, DSHB, deposited by Corey Goodman) (Patel, Snow, & Goodman, 1987). Alexa488, Alexa548, Alexa564 and Alexa633-conjugated secondary antibodies (Thermo Fisher Scientific) were used at a dilution of 1:500.

Adult wing preparation

The left wings from female flies were dissected and mounted on slides using Canada balsam (Benz Microscope, BB0020) as previously described (Takemura & Adachi-Yamada, 2011). Images were taken using a ZEISS Stemi SV 11 microscope equipped with a Jenoptic ProgRes C3 digital camera.

Acknowledgements

We thank Melissa Harrison, Kate O'Connor-Giles, Jill Wildonger, Gary Struhl, Scott Selleck, Hugo Bellen, the Bloomington Drosophila Stock Center (NIH P40OD018537), the Transgenic RNAi Project at Harvard Medical School [NIH/NIGMS R01-GM08947], and the Drosophila Genomics Resource Center (NIH 2P40OD010949) for sharing fly strains and plasmids. We also thank the Proteomics Core Facility at the Sahlgrenska Academy, University of Gothenburg, Sweden for running all the MS analyses. This work was supported by the National Institutes of Health (R01 GM115099) to H.N. M.T. held postdoctoral fellowships from the Japan Society for the Promotion of Science and the Uehara Memorial Foundation.

Competing interests

The authors declare no competing or financial interests.

References

Akiyama, T., Kamimura, K., Firkus, C., Takeo, S., Shimmi, O., & Nakato, H. (2008). Dally regulates Dpp morphogen gradient formation by stabilizing Dpp on the cell surface. *Developmental Biology*, *313*(1), 408–419. http://doi.org/10.1016/j.ydbio.2007.10.035

Baena-Lopez, L. A., Nojima, H., & Vincent, J.-P. (2012). Integration of morphogen signalling within the growth regulatory network. *Current Opinion in Cell Biology*, *24*(2), 166–172. http://doi.org/10.1016/j.ceb.2011.12.010

Bandtlow, C. E., & Zimmermann, D. R. (2000). Proteoglycans in the developing brain: new conceptual insights for old proteins. *Physiological Reviews*, *80*(4), 1267–1290. http://doi.org/10.1152/physrev.2000.80.4.1267

Bech-Hansen, N. T., Naylor, M. J., Maybaum, T. A., Sparkes, R. L., Koop, B., Birch, D. G., et al. (2000). Mutations in NYX, encoding the leucine-rich proteoglycan nyctalopin, cause X-linked complete congenital stationary night blindness. *Nature Genetics*, *26*(3), 319–323. http://doi.org/10.1038/81619

Bischof, J., Maeda, R. K., Hediger, M., Karch, F., & Basler, K. (2007). An optimized transgenesis system for Drosophila using germ-line-specific phiC31 integrases. *Proceedings of the National Academy of Sciences of the United States of America*, *104*(9), 3312–3317. http://doi.org/10.1073/pnas.0611511104

Briscoe, J., & Thérond, P. P. (2013). The mechanisms of Hedgehog signalling and its roles in development and disease. *Nature Reviews. Molecular Cell Biology*, *14*(7), 416–429. http://doi.org/10.1038/nrm3598

Calleja, M., Moreno, E., Pelaz, S., & Morata, G. (1996). Visualization of gene expression in living adult Drosophila. *Science (New York, NY)*, *274*(5285), 252–255.

Campbell, G., Göring, H., Lin, T., Spana, E., Andersson, S., Doe, C. Q., & Tomlinson, A. (1994). RK2, a glial-specific homeodomain protein required for embryonic nerve cord condensation and viability in Drosophila. *Development (Cambridge, England)*, *120*(10), 2957–2966.

Capdevila, J., & Guerrero, I. (1994). Targeted expression of the signaling molecule decapentaplegic induces pattern duplications and growth alterations in Drosophila wings. *The EMBO Journal*, *13*(19), 4459–4468.

Capdevila, J., Pariente, F., Sampedro, J., Alonso, J. L., & Guerrero, I. (1994). Subcellular localization of the segment polarity protein patched suggests an interaction with the wingless reception complex in Drosophila embryos. *Development (Cambridge, England)*, *120*(4), 987–998.

Coles, C. H., Shen, Y., Tenney, A. P., Siebold, C., Sutton, G. C., Lu, W., et al. (2011). Proteoglycan-specific molecular switch for RPTPσ clustering and neuronal extension. *Science (New York, NY)*, *332*(6028), 484–488. http://doi.org/10.1126/science.1200840

Cortes, M., Baria, A. T., & Schwartz, N. B. (2009). Sulfation of chondroitin sulfate proteoglycans is necessary for proper Indian hedgehog signaling in the developing growth plate. *Development (Cambridge, England)*, *136*(10), 1697–1706. http://doi.org/10.1242/dev.030742

Denef, N., Neubüser, D., Perez, L., & Cohen, S. M. (2000). Hedgehog induces opposite changes in turnover and subcellular localization of patched and smoothened. *Cell*, *102*(4), 521–531.

Desbordes, S. C., & Sanson, B. (2003). The glypican Dally-like is required for Hedgehog signalling in the embryonic epidermis of Drosophila. *Development (Cambridge, England)*, *130*(25), 6245–6255. http://doi.org/10.1242/dev.00874

Duncan, D. M., Burgess, E. A., & Duncan, I. (1998). Control of distal antennal identity and tarsal development in Drosophila by spineless-aristapedia, a homolog of the mammalian dioxin receptor. *Genes & Development*, *12*(9), 1290–1303.

Esko, J. D., & Zhang, L. (1996). Influence of core protein sequence on glycosaminoglycan assembly. *Current Opinion in Structural Biology*, *6*(5), 663–670.

Gradilla, A.-C., & Guerrero, I. (2013). Hedgehog on the move: a precise spatial control of Hedgehog dispersion shapes the gradient. *Current Opinion in Genetics & Development*, *23*(4), 363–373. http://doi.org/10.1016/j.gde.2013.04.011

533 Gratz, S. J., Cummings, A. M., Nguyen, J. N., Hamm, D. C., Donohue, L. K., Harrison, M. M., et al.
534 (2013). Genome engineering of Drosophila with the CRISPR RNA-guided Cas9 nuclease. *Genetics*,
535 *194*(4), 1029–1035. http://doi.org/10.1534/genetics.113.152710
536 Gratz, S. J., Ukken, F. P., Rubinstein, C. D., Thiede, G., Donohue, L. K., Cummings, A. M., & O'Connor-
537 Giles, K. M. (2014). Highly specific and efficient CRISPR/Cas9-catalyzed homology-directed repair
538 in Drosophila. *Genetics*, *196*(4), 961–971. http://doi.org/10.1534/genetics.113.160713
539 Groth, A. C., Fish, M., Nusse, R., & Calos, M. P. (2004). Construction of transgenic Drosophila by using
540 the site-specific integrase from phage phiC31. *Genetics*, *166*(4), 1775–1782.
541 Hartl, T. A., & Scott, M. P. (2014). Wing tips: The wing disc as a platform for studying Hedgehog
542 signaling. *Methods*, *68*(1), 199–206. http://doi.org/10.1016/j.ymeth.2014.02.002
543 Hayashi, S., Ito, K., Sado, Y., Taniguchi, M., Akimoto, A., Takeuchi, H., et al. (2002). GETDB, a
544 database compiling expression patterns and molecular locations of a collection of Gal4 enhancer
545 traps. *Genesis (New York, NY : 2000)*, *34*(1-2), 58–61. http://doi.org/10.1002/gene.10137
546 Hayashi, Y., Sexton, T. R., Dejima, K., Perry, D. W., Takemura, M., Kobayashi, S., et al. (2012).
547 Glypicans regulate JAK/STAT signaling and distribution of the Unpaired morphogen. *Development*
548 *(Cambridge, England)*, *139*(22), 4162–4171. http://doi.org/10.1242/dev.078055
549 Holt, C. E., & Dickson, B. J. (2005). Sugar Codes for Axons? *Neuron*, *46*(2), 169–172.
550 http://doi.org/10.1016/j.neuron.2005.03.021
551 Hu, Y., Flockhart, I., Vinayagam, A., Bergwitz, C., Berger, B., Perrimon, N., & Mohr, S. E. (2011). An
552 integrative approach to ortholog prediction for disease-focused and other functional studies. *BMC*
553 *Bioinformatics*, *12*(1), 357. http://doi.org/10.1186/1471-2105-12-357
554 Huff, J. L., Kingsley, K. L., Miller, J. M., & Hoshizaki, D. K. (2002). Drosophila windpipe codes for a
555 leucine-rich repeat protein expressed in the developing trachea. *Mechanisms of Development*, *111*(1-
556 2), 173–176.
557 Jia, J., Tong, C., Wang, B., Luo, L., & Jiang, J. (2004). Hedgehog signalling activity of Smoothened
558 requires phosphorylation by protein kinase A and casein kinase I. *Nature*, *432*(7020), 1045–1050.
559 http://doi.org/10.1038/nature03179
560 Kantor, D. B., Chivatakarn, O., Peer, K. L., Oster, S. F., Inatani, M., Hansen, M. J., et al. (2004).
561 Semaphorin 5A is a bifunctional axon guidance cue regulated by heparan and chondroitin sulfate
562 proteoglycans. *Neuron*, *44*(6), 961–975. http://doi.org/10.1016/j.neuron.2004.12.002
563 Kim, M.-S., Saunders, A. M., Hamaoka, B. Y., Beachy, P. A., & Leahy, D. J. (2011). Structure of the
564 protein core of the glypican Dally-like and localization of a region important for hedgehog signaling.
565 *Proceedings of the National Academy of Sciences of the United States of America*, *108*(32), 13112–
566 13117. http://doi.org/10.1073/pnas.1109877108
567 Kudo, A., Shigenobu, S., Kadota, K., Nozawa, M., Shibata, T. F., Ishikawa, Y., & Matsuo, T. (2017).
568 Comparative analysis of the brain transcriptome in a hyper-aggressive fruit fly, Drosophila
569 prolongata. *Insect Biochemistry and Molecular Biology*, *82*, 11–20.
570 http://doi.org/10.1016/j.ibmb.2017.01.006
571 Lander, A. D., & Selleck, S. B. (2000). The elusive functions of proteoglycans: in vivo veritas. *The*
572 *Journal of Cell Biology*, *148*(2), 227–232.
573 Lee, J. J., Kessler, von, D. P., Parks, S., & Beachy, P. A. (1992). Secretion and localized transcription
574 suggest a role in positional signaling for products of the segmentation gene hedgehog. *Cell*, *71*(1),
575 33–50.
576 Lee, J.-S., & Chien, C.-B. (2004). When sugars guide axons: insights from heparan sulphate proteoglycan
577 mutants. *Nature Reviews Genetics*, *5*(12), 923–935. http://doi.org/10.1038/nrg1490
578 Lin, D. M., & Goodman, C. S. (1994). Ectopic and increased expression of Fasciclin II alters motoneuron
579 growth cone guidance. *Neuron*, *13*(3), 507–523.
580 Lindahl, U., & Li, J.-P. (2009). Interactions between heparan sulfate and proteins-design and functional
581 implications. *International Review of Cell and Molecular Biology*, *276*, 105–159.
582 http://doi.org/10.1016/S1937-6448(09)76003-4

583 Lu, J., Wang, D., & Shen, J. (2017). Hedgehog signalling is required for cell survival in Drosophila wing
584 pouch cells. *Scientific Reports*, *7*(1), 11317. http://doi.org/10.1038/s41598-017-10550-4
585 Lum, L., Yao, S., Mozer, B., Rovescalli, A., Kessler, Von, D., Nirenberg, M., & Beachy, P. A. (2003a).
586 Identification of Hedgehog pathway components by RNAi in Drosophila cultured cells. *Science (New*
587 *York, NY)*, *299*(5615), 2039–2045. http://doi.org/10.1126/science.1081403
588 Lum, L., Zhang, C., Oh, S., Mann, R. K., Kessler, von, D. P., Taipale, J., et al. (2003b). Hedgehog signal
589 transduction via Smoothened association with a cytoplasmic complex scaffolded by the atypical
590 kinesin, Costal-2. *Molecular Cell*, *12*(5), 1261–1274.
591 Matsumoto, Y., Irie, F., Inatani, M., Tessier-Lavigne, M., & Yamaguchi, Y. (2007). Netrin-1/DCC
592 signaling in commissural axon guidance requires cell-autonomous expression of heparan sulfate. *The*
593 *Journal of Neuroscience : the Official Journal of the Society for Neuroscience*, *27*(16), 4342–4350.
594 http://doi.org/10.1523/JNEUROSCI.0700-07.2007
595 Momota, R., Naito, I., Ninomiya, Y., & Ohtsuka, A. (2011). Drosophila type XV/XVIII collagen, Mp, is
596 involved in Wingless distribution. *Matrix Biology : Journal of the International Society for Matrix*
597 *Biology*, *30*(4), 258–266. http://doi.org/10.1016/j.matbio.2011.03.008
598 Motzny, C. K., & Holmgren, R. (1995). The Drosophila cubitus interruptus protein and its role in the
599 wingless and hedgehog signal transduction pathways. *Mechanisms of Development*, *52*(1), 137–150.
600 Mullor, J. L., Calleja, M., Capdevila, J., & Guerrero, I. (1997). Hedgehog activity, independent of
601 decapentaplegic, participates in wing disc patterning. *Development (Cambridge, England)*, *124*(6),
602 1227–1237.
603 Nakato, H., & Li, J.-P. (2016). Functions of Heparan Sulfate Proteoglycans in Development: Insights
604 From Drosophila Models. *International Review of Cell and Molecular Biology*, *325*, 275–293.
605 http://doi.org/10.1016/bs.ircmb.2016.02.008
606 Nern, A., Pfeiffer, B. D., & Rubin, G. M. (2015). Optimized tools for multicolor stochastic labeling reveal
607 diverse stereotyped cell arrangements in the fly visual system. *Proceedings of the National Academy*
608 *of Sciences of the United States of America*, *112*(22), E2967–76.
609 http://doi.org/10.1073/pnas.1506763112
610 Noborn, F., Gomez Toledo, A., Green, A., Nasir, W., Sihlbom, C., Nilsson, J., & Larson, G. (2016). Site-
611 specific identification of heparan and chondroitin sulfate glycosaminoglycans in hybrid
612 proteoglycans. *Scientific Reports*, *6*(1), 34537. http://doi.org/10.1038/srep34537
613 Noborn, F., Gomez Toledo, A., Nasir, W., Nilsson, J., Dierker, T., Kjellén, L., & Larson, G. (2018).
614 Expanding the chondroitin glycoproteome of Caenorhabditis elegans. *Journal of Biological*
615 *Chemistry*, *293*(1), 379–389. http://doi.org/10.1074/jbc.M117.807800
616 Noborn, F., Gomez Toledo, A., Sihlbom, C., Lengqvist, J., Fries, E., Kjellén, L., et al. (2015).
617 Identification of chondroitin sulfate linkage region glycopeptides reveals prohormones as a novel
618 class of proteoglycans. *Molecular & Cellular Proteomics : MCP*, *14*(1), 41–49.
619 http://doi.org/10.1074/mcp.M114.043703
620 Nolo, R., Abbott, L. A., & Bellen, H. J. (2000). Senseless, a Zn finger transcription factor, is necessary
621 and sufficient for sensory organ development in Drosophila. *Cell*, *102*(3), 349–362.
622 O'Keefe, D. D., Thor, S., & Thomas, J. B. (1998). Function and specificity of LIM domains in Drosophila
623 nervous system and wing development. *Development (Cambridge, England)*, *125*(19), 3915–3923.
624 Olson, S. K., Bishop, J. R., Yates, J. R., Oegema, K., & Esko, J. D. (2006). Identification of novel
625 chondroitin proteoglycans in Caenorhabditis elegans: embryonic cell division depends on CPG-1 and
626 CPG-2. *The Journal of Cell Biology*, *173*(6), 985–994. http://doi.org/10.1083/jcb.200603003
627 Patel, N. H., Martín-Blanco, E., Coleman, K. G., Poole, S. J., Ellis, M. C., Kornberg, T. B., & Goodman,
628 C. S. (1989). Expression of engrailed proteins in arthropods, annelids, and chordates. *Cell*, *58*(5),
629 955–968.
630 Patel, N. H., Snow, P. M., & Goodman, C. S. (1987). Characterization and cloning of fasciclin III: a
631 glycoprotein expressed on a subset of neurons and axon pathways in Drosophila. *Cell*, *48*(6), 975–
632 988.

633 Perrimon, N., & Bernfield, M. (2000). Specificities of heparan sulphate proteoglycans in developmental
634 processes. *Nature*, *404*(6779), 725–728. http://doi.org/10.1038/35008000
635 Pfeiffer, B. D., Ngo, T.-T. B., Hibbard, K. L., Murphy, C., Jenett, A., Truman, J. W., & Rubin, G. M.
636 (2010). Refinement of tools for targeted gene expression in Drosophila. *Genetics*, *186*(2), 735–755.
637 http://doi.org/10.1534/genetics.110.119917
638 Poulain, F. E., & Yost, H. J. (2015). Heparan sulfate proteoglycans: a sugar code for vertebrate
639 development? *Development (Cambridge, England)*, *142*(20), 3456–3467.
640 http://doi.org/10.1242/dev.098178
641 Pusch, C. M., Zeitz, C., Brandau, O., Pesch, K., Achatz, H., Feil, S., et al. (2000). The complete form of
642 X-linked congenital stationary night blindness is caused by mutations in a gene encoding a leucine-
643 rich repeat protein. *Nature Genetics*, *26*(3), 324–327. http://doi.org/10.1038/81627
644 Ragkousi, K., & Gibson, M. C. (2014). Cell division and the maintenance of epithelial order. *The Journal*
645 *of Cell Biology*, *207*(2), 181–188. http://doi.org/10.1083/jcb.201408044
646 Ren, W., Zhang, Y., Li, M., Wu, L., Wang, G., Baeg, G.-H., et al. (2015). Windpipe controls Drosophila
647 intestinal homeostasis by regulating JAK/STAT pathway via promoting receptor endocytosis and
648 lysosomal degradation. *PLoS Genetics*, *11*(4), e1005180.
649 http://doi.org/10.1371/journal.pgen.1005180
650 Ren, X., Yang, Z., Xu, J., Sun, J., Mao, D., Hu, Y., et al. (2014). Enhanced specificity and efficiency of
651 the CRISPR/Cas9 system with optimized sgRNA parameters in Drosophila. *CellReports*, *9*(3), 1151–
652 1162. http://doi.org/10.1016/j.celrep.2014.09.044
653 Riggleman, B., Schedl, P., & Wieschaus, E. (1990). Spatial expression of the Drosophila segment polarity
654 gene armadillo is posttranscriptionally regulated by wingless. *Cell*, *63*(3), 549–560.
655 Saied-Santiago, K., & Bülow, H. E. (2018). Diverse roles for glycosaminoglycans in neural patterning.
656 *Developmental Dynamics : an Official Publication of the American Association of Anatomists*,
657 *247*(1), 54–74. http://doi.org/10.1002/dvdy.24555
658 Schaefer, L., & Iozzo, R. V. (2008). Biological functions of the small leucine-rich proteoglycans: from
659 genetics to signal transduction. *The Journal of Biological Chemistry*, *283*(31), 21305–21309.
660 http://doi.org/10.1074/jbc.R800020200
661 Schindelin, J., Arganda-Carreras, I., Frise, E., Kaynig, V., Longair, M., Pietzsch, T., et al. (2012). Fiji: an
662 open-source platform for biological-image analysis. *Nature Methods*, *9*(7), 676–682.
663 http://doi.org/10.1038/nmeth.2019
664 Silver, J., & Miller, J. H. (2004). Regeneration beyond the glial scar. *Nature Reviews Neuroscience*, *5*(2),
665 146–156. http://doi.org/10.1038/nrn1326
666 Smith, R. B., Machamer, J. B., Kim, N. C., Hays, T. S., & Marques, G. (2012). Relay of retrograde
667 synaptogenic signals through axonal transport of BMP receptors. *Journal of Cell Science*, *125*(Pt 16),
668 3752–3764. http://doi.org/10.1242/jcs.094292
669 Strigini, M., & Cohen, S. M. (1997). A Hedgehog activity gradient contributes to AP axial patterning of
670 the Drosophila wing. *Development (Cambridge, England)*, *124*(22), 4697–4705.
671 Tabata, T., & Takei, Y. (2004). Morphogens, their identification and regulation. *Development*
672 *(Cambridge, England)*, *131*(4), 703–712. http://doi.org/10.1242/dev.01043
673 Takei, Y. (2004). Three Drosophila EXT genes shape morphogen gradients through synthesis of heparan
674 sulfate proteoglycans, *131*(1), 73–82. http://doi.org/10.1242/dev.00913
675 Takemura, M., & Adachi-Yamada, T. (2011). Cell death and selective adhesion reorganize the
676 dorsoventral boundary for zigzag patterning of Drosophila wing margin hairs. *Developmental*
677 *Biology*, *357*(2), 336–346. http://doi.org/10.1016/j.ydbio.2011.07.007
678 Takemura, M., & Nakato, H. (2015). Genetic approaches in the study of heparan sulfate functions in
679 Drosophila. *Methods in Molecular Biology (Clifton, N.J.)*, *1229*(Chapter 38), 497–505.
680 http://doi.org/10.1007/978-1-4939-1714-3_38
681 Takemura, M., & Nakato, H. (2017). Drosophila Sulf1 is required for the termination of intestinal stem
682 cell division during regeneration. *Journal of Cell Science*, *130*(2), 332–343.
683 http://doi.org/10.1242/jcs.195305

Tanimoto, H., Itoh, S., Dijke, ten, P., & Tabata, T. (2000). Hedgehog creates a gradient of DPP activity in Drosophila wing imaginal discs. *Molecular Cell*, *5*(1), 59–71.

Tavsanli, B. C., Ostrin, E. J., Burgess, H. K., Middlebrooks, B. W., Pham, T. A., & Mardon, G. (2004). Structure-function analysis of the Drosophila retinal determination protein Dachshund. *Developmental Biology*, *272*(1), 231–247. http://doi.org/10.1016/j.ydbio.2004.05.005

Townley, R. A., & Bülow, H. E. (2018). Deciphering functional glycosaminoglycan motifs in development. *Current Opinion in Structural Biology*, *50*, 144–154. http://doi.org/10.1016/j.sbi.2018.03.011

Toyoda, H., Kinoshita-Toyoda, A., & Selleck, S. B. (2000). Structural analysis of glycosaminoglycans in Drosophila and Caenorhabditis elegans and demonstration that tout-velu, a Drosophila gene related to EXT tumor suppressors, affects heparan sulfate in vivo. *The Journal of Biological Chemistry*, *275*(4), 2269–2275.

Van Vactor, D., Wall, D. P., & Johnson, K. G. (2006). Heparan sulfate proteoglycans and the emergence of neuronal connectivity. *Current Opinion in Neurobiology*, *16*(1), 40–51. http://doi.org/10.1016/j.conb.2006.01.011

Viswanathan, S., Williams, M. E., Bloss, E. B., Stasevich, T. J., Speer, C. M., Nern, A., et al. (2015). High-performance probes for light and electron microscopy. *Nature Methods*, *12*(6), 568–576. http://doi.org/10.1038/nmeth.3365

Wang, J., Al-Ouran, R., Hu, Y., Kim, S.-Y., Wan, Y.-W., Wangler, M. F., et al. (2017). MARRVEL: Integration of Human and Model Organism Genetic Resources to Facilitate Functional Annotation of the Human Genome. *American Journal of Human Genetics*. http://doi.org/10.1016/j.ajhg.2017.04.010

Wang, L., Dankert, H., Perona, P., & Anderson, D. J. (2008). A common genetic target for environmental and heritable influences on aggressiveness in Drosophila. *Proceedings of the National Academy of Sciences of the United States of America*, *105*(15), 5657–5663. http://doi.org/10.1073/pnas.0801327105

Whalen, D. M., Malinauskas, T., Gilbert, R. J. C., & Siebold, C. (2013). Structural insights into proteoglycan-shaped Hedgehog signaling. *Proceedings of the National Academy of Sciences of the United States of America*, *110*(41), 16420–16425. http://doi.org/10.1073/pnas.1310097110

Williams, E. H., Pappano, W. N., Saunders, A. M., Kim, M.-S., Leahy, D. J., & Beachy, P. A. (2010). Dally-like core protein and its mammalian homologues mediate stimulatory and inhibitory effects on Hedgehog signal response. *Proceedings of the National Academy of Sciences of the United States of America*, *107*(13), 5869–5874. http://doi.org/10.1073/pnas.1001777107

Xu, D., & Esko, J. D. (2014). Demystifying heparan sulfate-protein interactions. *Annual Review of Biochemistry*, *83*(1), 129–157. http://doi.org/10.1146/annurev-biochem-060713-035314

Xu, T., & Rubin, G. M. (1993). Analysis of genetic mosaics in developing and adult Drosophila tissues. *Development (Cambridge, England)*, *117*(4), 1223–1237.

Yan, D., Wu, Y., Yang, Y., Belenkaya, T. Y., Tang, X., & Lin, X. (2010). The cell-surface proteins Dally-like and Ihog differentially regulate Hedgehog signaling strength and range during development. *Development (Cambridge, England)*, *137*(12), 2033–2044. http://doi.org/10.1242/dev.045740

Zecca, M., Basler, K., & Struhl, G. (1995). Sequential organizing activities of engrailed, hedgehog and decapentaplegic in the Drosophila wing. *Development (Cambridge, England)*, *121*(8), 2265–2278.

Zecca, M., Basler, K., & Struhl, G. (1996). Direct and long-range action of a wingless morphogen gradient. *Cell*, *87*(5), 833–844. http://doi.org/10.5167/uzh-996

Zhang, F., McLellan, J. S., Ayala, A. M., Leahy, D. J., & Linhardt, R. J. (2007). Kinetic and structural studies on interactions between heparin or heparan sulfate and proteins of the hedgehog signaling pathway. *Biochemistry*, *46*(13), 3933–3941. http://doi.org/10.1021/bi6025424

Zhu, A. J., Zheng, L., Suyama, K., & Scott, M. P. (2003). Altered localization of Drosophila Smoothened protein activates Hedgehog signal transduction. *Genes & Development*, *17*(10), 1240–1252. http://doi.org/10.1101/gad.1080803

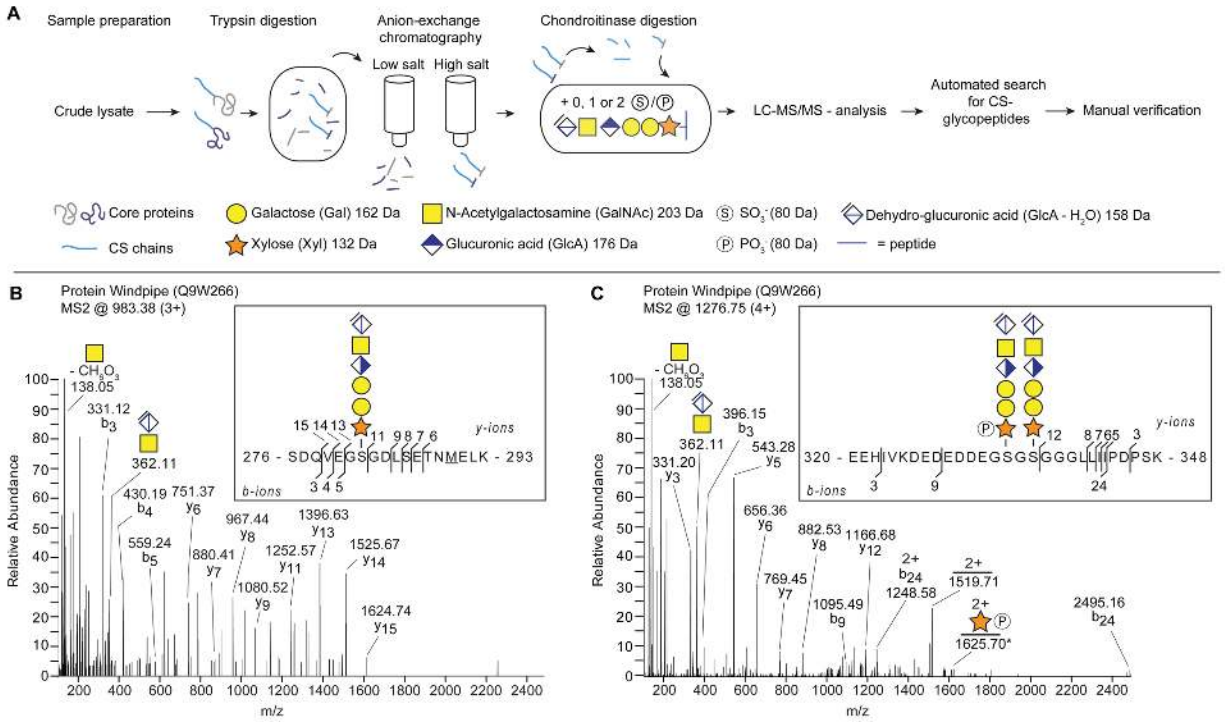

Figure 1. Identification of Wdp as a novel CSPG in *Drosophila*. (**A**) A scheme for identifying CSPGs in *Drosophila*. The workflow includes the enrichment of proteoglycans from fly extract, enzymatic hydrolysis and subsequent analysis and interpretation of mass spectra. (**B** and **C**) MS2 fragment mass spectra of Wdp protein (UniProt: Q9W266) showing two unique CS-glycopeptides. (B) Peptide (SDQVEGSGDLSETNMELK) identified with one hexasaccharide structure and one methionine oxidation (*m/z* 983.38; 3+) (C) Peptide (EEHIVKDEDEDDEGSGSGGGLLIIPDPSK) identified with two hexasaccharide structures where one of the hexasaccharides were modified with one phosphate modification (*m/z* 1276.76; 4+). The asterisk denotes the second isotopic peak.

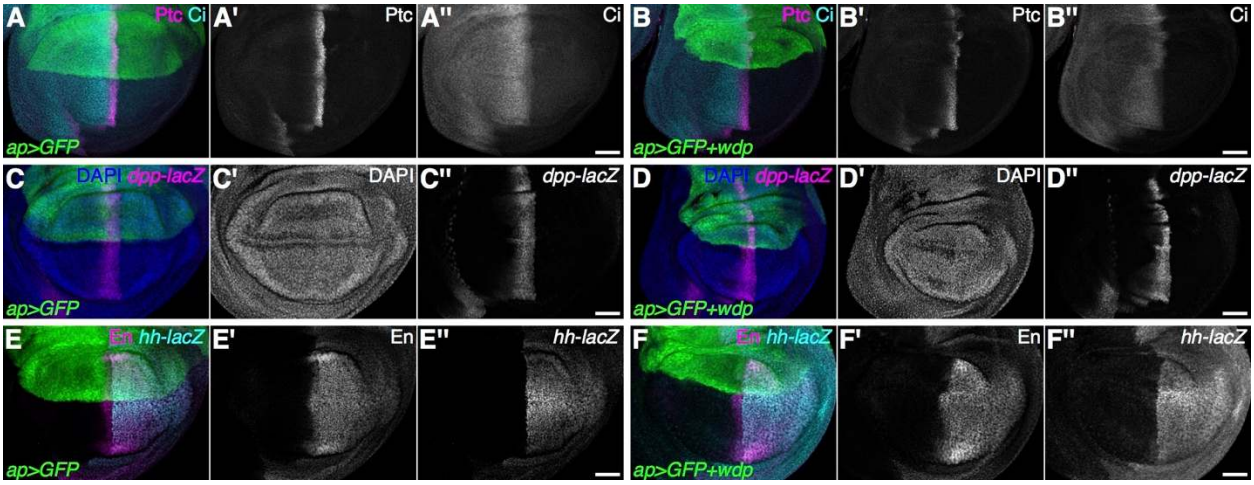

Figure 2. Overexpression of *wdp* reduces the Hh-signaling-active domain. (**A**–**F**) Control wing discs (A, C, and E) and wing discs overexpressing *wdp* with *ap-GAL4* (*ap>GFP+wdp*) (B, D, and F) were immunostained for the expression of Ptc, Ci (A and B), *dpp-lacZ* (C and D), En, and *hh-lacZ* (E and F). The expression domains of Ptc, Ci, and *dpp-lacZ* were reduced by *wdp* overexpression in the dorsal compartment compared to those in the ventral compartment. En expression induced by high-level Hh signaling in the anterior compartment is diminished by *wdp* overexpression. Note that the *hh-lacZ* expression is not affected by *wdp* overexpression. Nuclei were stained with DAPI (C and D). Anterior to the left; dorsal to the top. Scale bars: 50 μm.

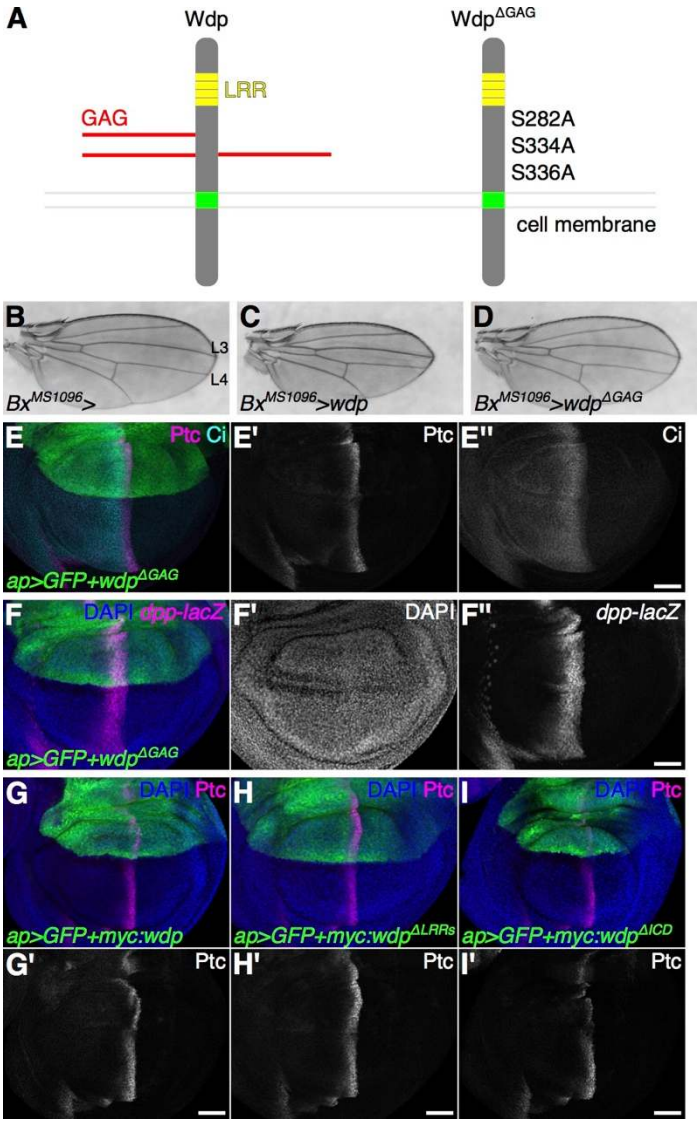

Figure 3. Wdp negatively regulates Hh signaling in a GAG-dependent manner. (**A**) A schematic drawing of wild-type Wdp and a mutant form of Wdp ($Wdp^{\Delta GAG}$). (**B**–**D**) A control adult wing (B) and adult wings expressing *UAS-wdp* (C) or *UAS-wdp*$^{\Delta GAG}$ (D) with *Bx*^{MS1096}*-GAL4*. (**E** and **F**) Wing discs expressing *UAS-wdp*$^{\Delta GAG}$ with *ap-GAL4* were immunostained for Ptc, Ci (E) and *dpp-lacZ* (F). (**G**–**I**) Wing discs expressing *UAS-3xMyc:wdp* (G), *UAS-3xMyc:wdp*$^{\Delta LRRs}$ (H), and *UAS-3xMyc:wdp*$^{\Delta ICD}$ (I) were immunostained for Ptc. Nuclei were stained with DAPI. Scale bars: 50 μm.

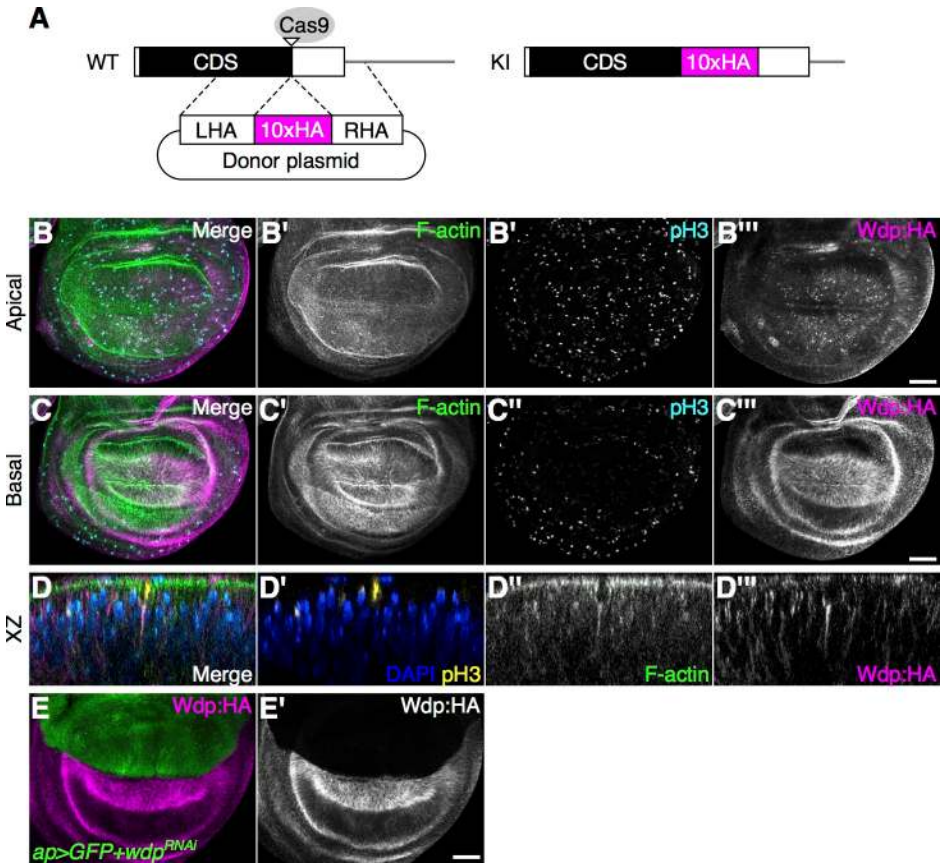

Figure 4. Wdp expression in the wing disc. (**A**) A schematic of CRISPR–Cas9-mediated gene editing of *wdp* for generating $wdp^{KI.HA}$. Ten copies of an HA epitope tag (smGFP-HA) were inserted in frame near the stop codon of the *wdp* coding sequence (CDS). Only the last exon is shown. CDS, the black box; smGFP-HA, the magenta box; LHA, left homology arm; RHA, right homology arm; Cas9 target site, the open triangle. (**B**–**D**) Wing discs homozygous for $wdp^{KI.HA}$ were stained with Alexa Fluor 568-conjugated phalloidin (F-actin), anti-phospho histone H3 antibody (pH3, mitotic nuclei), and anti-HA antibody. Apical (B) and basal (C) sections of the same disc are shown. Intense staining of Wdp:HA was observed on the basal side of wing disc epithelium (C–C'''). An optical cross section shows the accumulation of Wdp:HA in the basal projection of apically translocating mitotic cells (D–D'''). (**E**) Wdp:HA is not detectable in the dorsal compartment of a wing disc expressing wdp^{RNAi} (TRiP.HMC06302) with *ap-GAL4*. Nuclei were stained with DAPI (D and E). Scale bars: 50 μm.

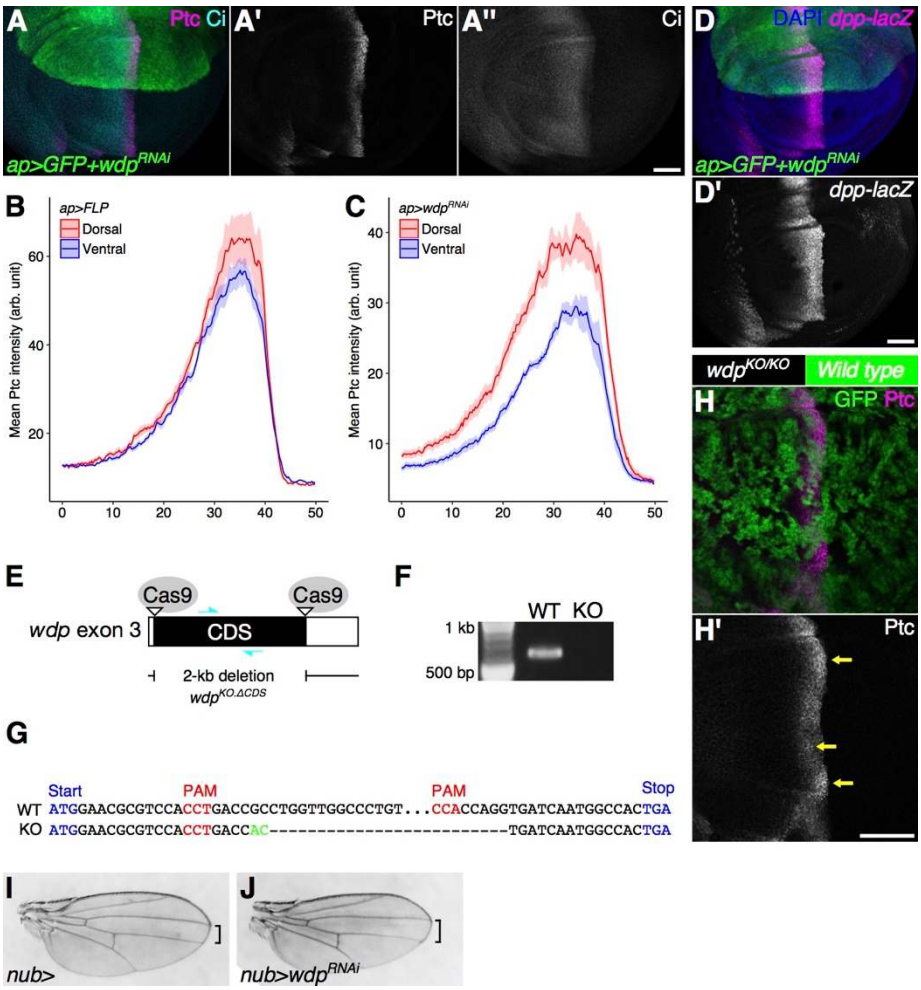

Figure 5. Loss of *wdp* leads to increased Hh signaling. (**A**) A wing disc expressing *UAS-wdp*^{RNAi} (TRiP.HMC06302) with *ap-GAL4* was immunostained for Ptc and Ci. (**B** and **C**) Signal intensity plots of the Ptc expression in the dorsal compartment (red) and ventral compartment (blue) in wing discs expressing *UAS-FLP* (B) or *UAS-wdp*^{RNAi} (C). Solid lines indicate the average intensity of Ptc staining and shaded areas show the standard error of the mean. (**D**) A wing disc expressing *UAS-wdp*^{RNAi} with *ap-GAL4* was immunostained for *dpp-lacZ*. Nuclei were stained with DAPI. (**E**) A schematic of the generation of a *wdp* loss-of-function allele (*wdp*$^{KO.\Delta CDS}$) lacking most of the *wdp* CDS using the CRISPR–Cas9 system. (**F**) A PCR-based genotyping result for the wild-type (WT) and *wdp*$^{KO.\Delta CDS}$ allele (KO) using a primer set shown as cyan arrows in E. (**G**) Genomic sequence of the *wdp* endogenous locus targeted by CRISPR–Cas9 to delete most of the *wdp* CDS. A small insertion is shown in green. (**H**) Somatic mosaic clones of *wdp*^{KO} were induced in the wing pouch using *nub-GAL4 UAS-FLP*. Homozygous *wdp*^{KO} mutant cells are marked by loss of GFP. Increased Ptc expression was observed in *wdp* mutant clones (yellow arrows) (**I**, **J**) A control adult wing (I) and a wing expressing *UAS-wdp*^{RNAi} (TRiP.HM05118) (J) by *nub-GAL4*. Scale bars: 50 μm.

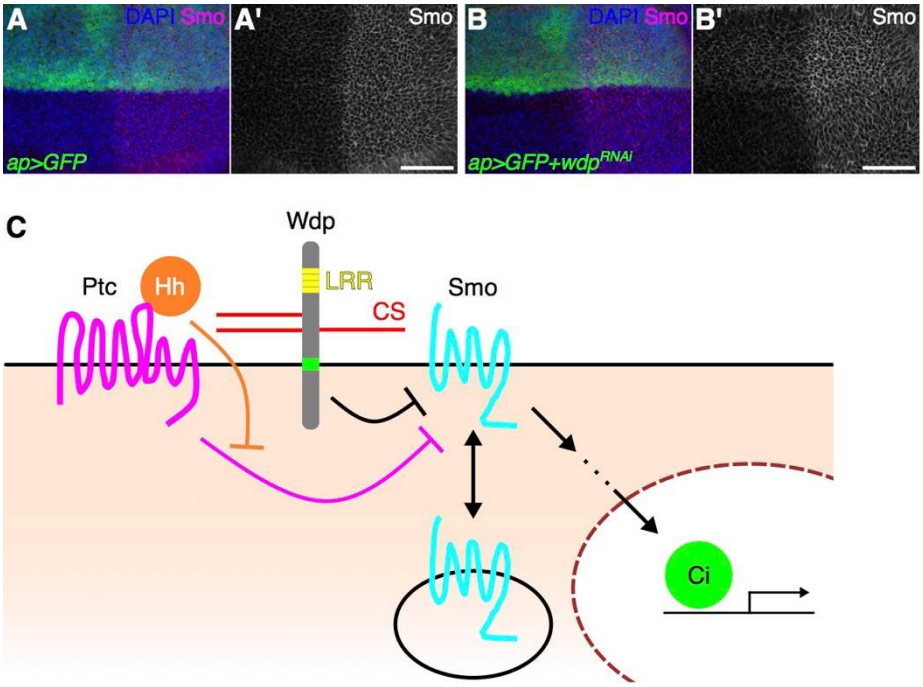

Figure 6. Wdp negatively regulates Smo cell surface accumulation. (**A**, **B**) A control wing disc and a wing disc expressing *UAS-wdp*^{RNAi} (TRiP.HMC06302) with *ap-GAL4* were immunostained for the expression of Smo. Nuclei were stained with DAPI. Scale bars: 50 μm. (**C**) A model for how Wdp modulates Hh signaling. Wdp inhibits Smo cell surface accumulation thereby reducing Hh signaling activity.

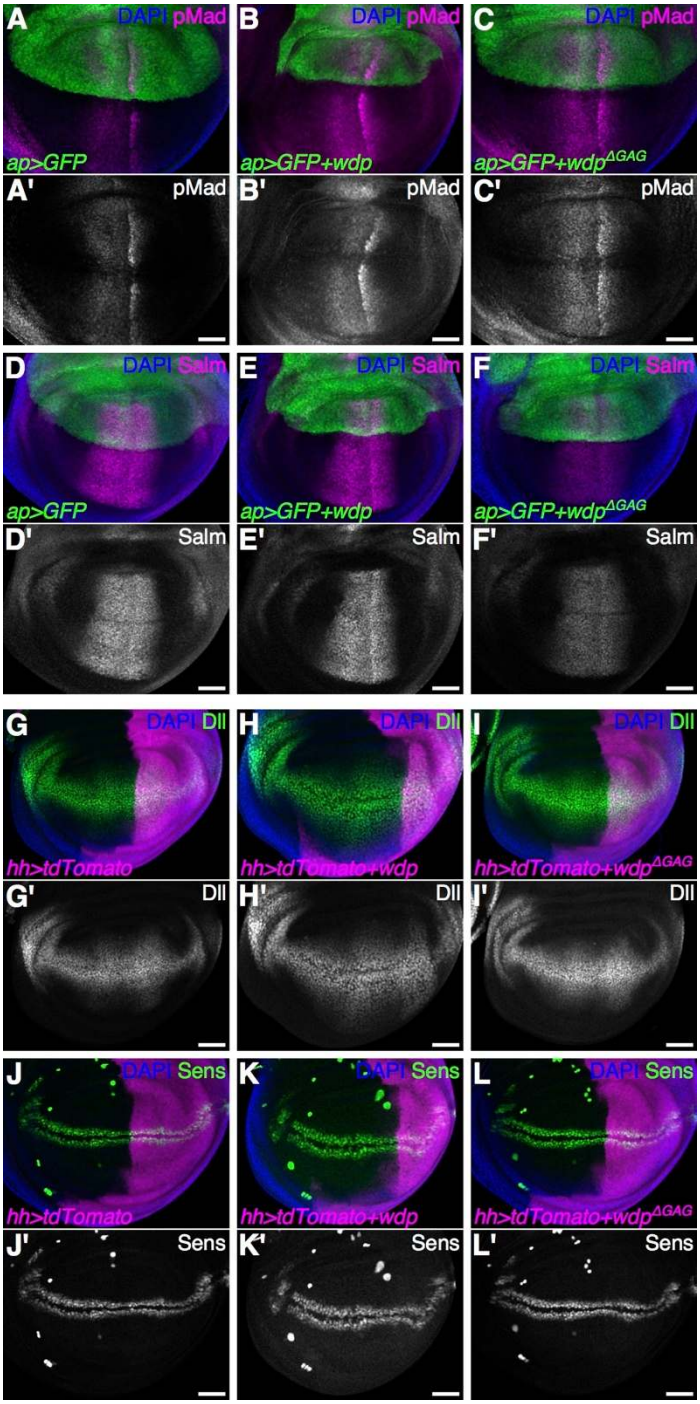

Figure S1. Effect of *wdp* overexpression on Dpp and Wg signaling. (**A**–**F**) Control wing discs (A and D) and wing discs expressing *UAS-wdp* (B and E) or *UAS-wdp*$^{\Delta GAG}$ (C and F) with *ap-GAL4* were immunostained for pMad (A–C) and Salm (D–F) as read-outs of Dpp signaling. (**G**–**L**) Control wing discs (G and J) and wing discs expressing *UAS-wdp* (H and K) or *UAS-wdp*$^{\Delta GAG}$ (I and L) with *hh-GAL4* were immunostained for Dll (G–I) and Sens (J–L) as read-outs of Wg signaling (Nolo et al., 2000; Zecca, Basler, & Struhl, 1996). Nuclei were stained with DAPI. Scale bars: 50 µm.

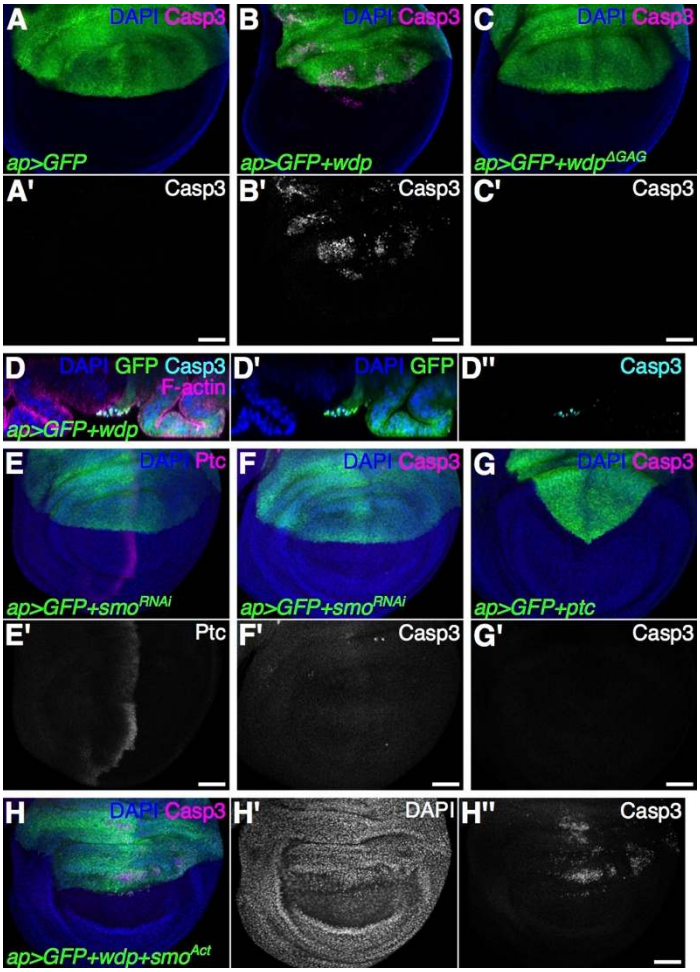

Figure S2. Overexpression of *wdp* in the wing disc induces apoptosis. (**A–C**) A control wing disc (A) and wing discs expressing *UAS-wdp* (B) or *UAS-wdp*$^{\Delta GAG}$ (C) with *ap-GAL4* were immunostained for cleaved Caspase-3 as a marker of apoptotic cells. (**D**) An optical cross section of a wing disc expressing *UAS-wdp* with *ap-GAL4*. Signals for cleaved Caspase-3 (cyan) and F-actin (magenta) are shown. (**E**) A wing disc expressing *UAS-smo*^{RNAi} (TRiP.HMC03577) with *ap-GAL4* was immunostained for Ptc. (**F** and **G**) Wing discs expressing *UAS-smo*^{RNAi} (F) or *UAS-ptc* (G) with *ap-GAL4* were immunostained for cleaved Caspase-3. (**H**) A wing disc coexpressing *UAS-wdp* and *UAS-FLAG:smo*^{Act} was immunostained for cleaved Caspase-3. Nuclei were stained with DAPI. Scale bars: 50 µm.

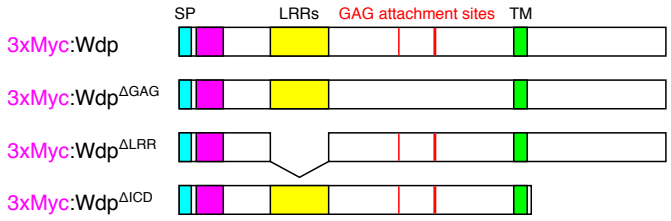

Figure S3. A schematic of 3xMyc-tagged wild-type and mutant Wdp constructs. The magenta box denotes 3 copies of a Myc tag. The cyan box indicates the signal peptide (SP). The yellow box shows the LRR motifs. The red line indicates the CS attachment sites. The green box shows the transmembrane domain (TM).

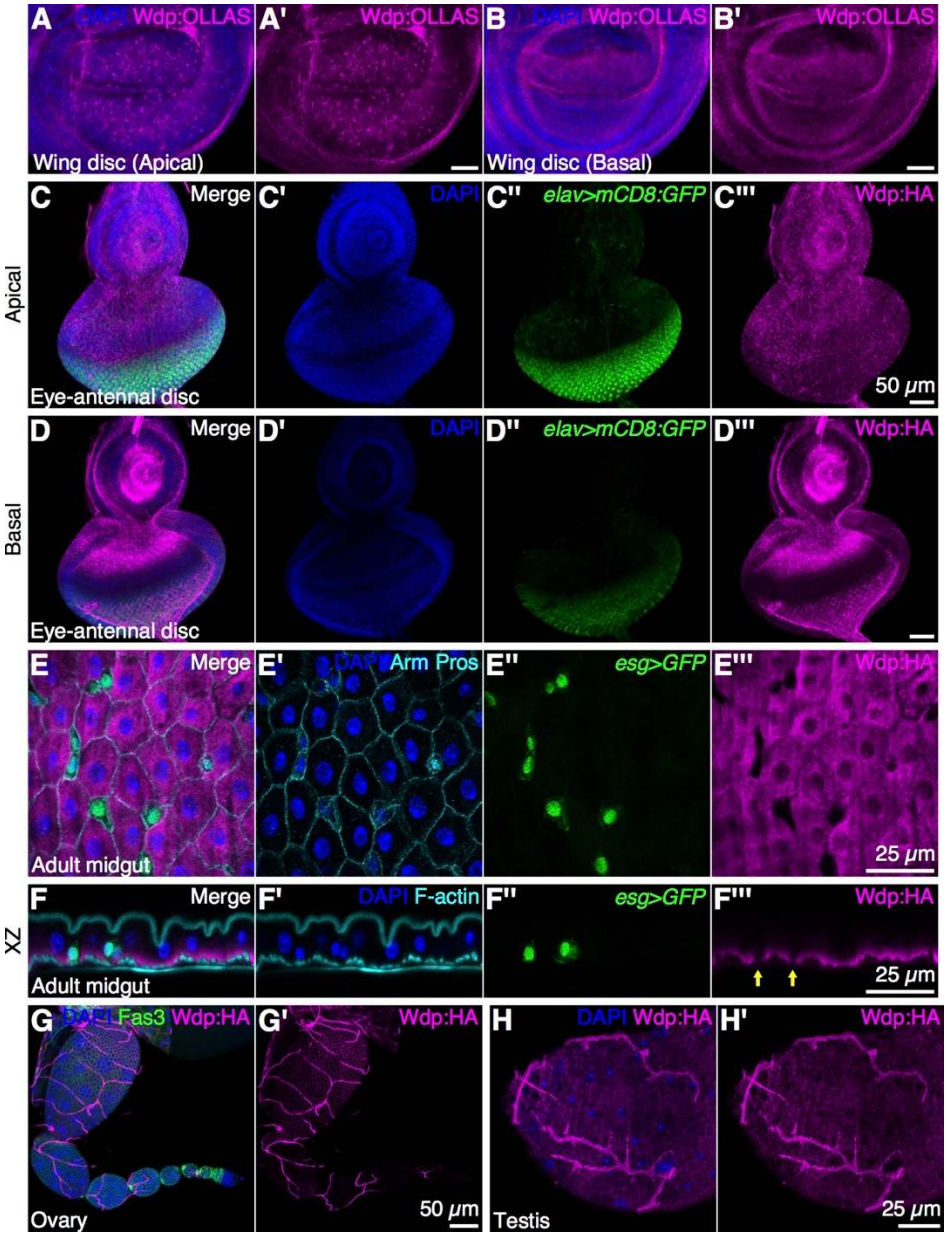

Figure S4. Expression patterns of Wdp in the eye disc, adult posterior midgut, ovary and testis. (**A**, **B**) Apical (A) and basal (B) sections of a wing disc homozygous for *wdp*$^{KI.OLLAS}$ was stained with anti-OLLAS antibody. (**C**–**H**) An eye disc, adult midgut, ovary, and testis with one or two copies of *wdp*$^{KI.HA}$ were immunostained with anti-HA antibody (magenta). (C, D) Apical (C) and basal (D) sections of an eye disc. Neurons are marked by *elav-GAL4 UAS-mCD8:GFP* (*elav>mCD8:GFP*, green). (E) An adult midgut showing ISCs/enteroblasts (*escargot-GAL4 UAS-GFP* [*esg>GFP*]), enteroendocrine cells (nuclear Prospero [Pros]), cell membrane (Armadillo [Arm]), and Wdp:HA. (F) An optical cross section of an adult midgut showing ISCs/enteroblasts (*esg>GFP*) and F-actin (stained by phalloidin-Alexa568). (G) Wdp:HA expression is detected in the egg chambers (stage 6 and later) in the ovary. Wdp:HA is also detectable in the tracheal system. (H) Wdp:HA expression is detected in the sheath cells and the tracheal system in the testis. Nuclei were stained with DAPI. Scale bars: 50 μm (A, B, C, D, and G), 25 μm (E, F, and H).

846 **Table S1. Genotypes of *Drosophila* strains used in each figure.**
847

Figure	Panel	Genotype
2	A	*ap-GAL4 UAS-GFP/+*
2	B	*ap-GAL4 UAS-GFP/+; UAS-wdp/+*
2	C	*ap-GAL4 UAS-GFP dpp-lacZ/+*
2	D	*ap-GAL4 UAS-GFP dpp-lacZ/+; UAS-wdp/+*
2	E	*ap-GAL4 UAS-GFP hh-lacZ/+*
2	F	*ap-GAL4 UAS-GFP hh-lacZ/+; UAS-wdp/+*
3	B	Bx^{MS1096}*-GAL4/+*
3	C	Bx^{MS1096}*-GAL4/+; UAS-wdp/+*
3	D	Bx^{MS1096}*-GAL4/+; UAS-wdp*$^{\Delta GAG}$
3	E	*ap-GAL4 UAS-GFP/+; UAS-wdp*$^{\Delta GAG}$*/+*
3	F	*ap-GAL4 UAS-GFP dpp-lacZ/+; UAS-wdp*$^{\Delta GAG}$*/+*
3	G	*ap-GAL4 UAS-GFP/+; UAS-3xMyc:wdp/+*
3	H	*ap-GAL4 UAS-GFP/+; UAS-3xMyc:wdp*$^{\Delta LRRs}$*/+*
3	I	*ap-GAL4 UAS-GFP/+; UAS-3xMyc:wdp*$^{\Delta ICD}$*/+*
4	B, C, D	*wdp*$^{KI.HA}$*/wdp*$^{KI.HA}$
4	E	*ap-GAL4 UAS-GFP wdp*$^{KI.HA}$*/UAS-wdp*$^{RNAi.HMC06302}$
5	A, C	*ap-GAL4 UAS-GFP/UAS-wdp*$^{RNAi.HMC06302}$
5	B	*ap-GAL4 UAS-GFP/UAS-wdp*$^{RNAi.HMC06302}$
5	D	*ap-GAL4 UAS-GFP dpp-lacZ/UAS-wdp*$^{RNAi.HMC06302}$
5	H	*nub-GAL4, FRT42D wdp*$^{KO.\ \Delta CDS}$*/FRT42D 2xubi-GFP; UAS-FLP/+*
5	I	*nub-GAL4/+*
5	J	*nub-GAL4/+; UAS-wdp*$^{RNAi.HMS05118}$*/+*
6	A	*ap-GAL4 UAS-GFP/+*
6	B	*ap-GAL4 UAS-GFP/UAS-wdp*$^{RNAi.HMC06302}$
S1	A, D	*ap-GAL4 UAS-GFP/+*
S1	B, E	*ap-GAL4 UAS-GFP/+; UAS-wdp/+*
S1	C, F	*ap-GAL4 UAS-GFP/+; UAS-wdp*$^{\Delta GAG}$*/+*
S1	G, J	*hh-GAL4 UAS-tdTomato/+*
S1	H, K	*hh-GAL4 UAS-tdTomato/UAS-wdp*
S1	I, L	*hh-GAL4 UAS-tdTomato/UAS-wdp*$^{\Delta GAG}$
S2	A, D	*ap-GAL4 UAS-GFP/+*
S2	B	*ap-GAL4 UAS-GFP/+; UAS-wdp/+*
S2	C	*ap-GAL4 UAS-GFP/+; UAS- wdp*$^{\Delta GAG}$*/+*
S2	E, F	*ap-GAL4 UAS-GFP/UAS-smo*$^{RNAi.HMC03577}$
S2	G	*ap-GAL4 UAS-GFP/UAS-ptc*
S2	H	*ap-GAL4 UAS-GFP/UAS-FLAG:smo*^{Act}*; UAS-wdp/+*
S4	A, B	*wdp*$^{KI.OLLAS}$*/wdp*$^{KI.OLLAS}$
S4	C, D	*elav-GAL4 UAS-mCD8:GFP/+; wdp*$^{KI.HA}$*/+*
S4	E, F	*esg-GAL4 UAS-GFP/+; wdp*$^{KI.HA}$*/+*
S4	G, H	*wdp*$^{KI.HA}$*/wdp*$^{KI.HA}$

848
849
850